Solar wind and heavy ion properties of interplanetary coronal mass ejections

Article

Published Version

www.reading.ac.uk/centaur

CrossMark

Solar Wind and Heavy Ion Properties of Interplanetary Coronal Mass Ejections

M.J. Owens[1] (ORCID)

Abstract Magnetic field and plasma properties of the solar wind measured in near-Earth space are a convolution of coronal source conditions and in-transit processes which take place between the corona and near-Earth space. Elemental composition and heavy ion charge states, however, are not significantly altered during transit to Earth and thus such properties can be used to diagnose the coronal source conditions of the solar wind observed *in situ*. We use data from the *Advanced Composition Explorer* (ACE) spacecraft to statistically quantify differences in the coronal source properties of interplanetary coronal mass ejections (ICMEs). Magnetic clouds, ICMEs which contain a magnetic flux-rope signature, display heavy ion properties consistent with significantly hotter coronal source regions than non-cloud ICMEs. Specifically, magnetic clouds display significantly elevated ion charge states, suggesting they receive greater heating in the low corona. Further dividing ICMEs by speed, however, shows this effect is primarily limited to fast magnetic clouds and that in terms of heavy ion properties, slow magnetic clouds are far more similar to non-cloud ICMEs. As such, fast magnetic clouds appear distinct from other ICME types in terms of both ion charge states and elemental composition. ICME speed, rather ICME type, correlates with helium abundance and iron charge state, consistent with fast ICMEs being heated through the more extended corona. Fast ICMEs also tend to be embedded within faster ambient solar wind than slow ICMEs, though this could be partly the result of in-transit drag effects. These signatures are discussed in terms of spatial sampling of ICMEs and from fundamentally different coronal formation and release processes.

Keywords Coronal mass ejections, interplanetary · Magnetic fields, interplanetary · Solar wind, disturbances · Solar wind, shock waves

✉ M.J. Owens
  m.j.owens@reading.ac.uk

[1] Space and Atmospheric Electricity Group, Department of Meteorology, University of Reading, Earley Gate, PO Box 243, Reading RG6 6BB, UK

Springer

1. Introduction

Coronal mass ejections (CMEs) are episodic eruptions of coronal plasma and magnetic flux, responsible for the largest space-weather disturbances (Gosling, 1993) and significant restructuring of the coronal magnetic field (Low, 2001; Luhmann *et al.*, 1999; Owens and Crooker, 2006). On the basis of *in situ* plasma and magnetic field observations, interplanetary CMEs (ICMEs) are observed to fall into two broad classes: magnetic clouds (Burlaga *et al.*, 1981), primarily characterised by a coherent rotation in the heliospheric magnetic field (HMF) direction interpreted as a magnetic flux rope (Lepping, Jones, and Burlaga, 1990), and non-cloud ICMEs, which have more complex or unstructured magnetic field signatures. It is unclear whether these different types of ICMEs are the result of different fundamental formation and release mechanisms back in the corona, or whether they are simply the result of different spatial sampling of large heliospheric structures (Riley *et al.*, 2006).

Part of the difficulty in interpreting ICME observations is that solar wind properties measured *in situ* are a convolution of solar wind formation processes with in-transit processes that occur between the Sun and observer. Compression, momentum transfer and heating mean that HMF, solar wind speed, density and temperature can all be modified in transit between the Sun and observer. For example, solar wind stream interaction regions (Pizzo, 1991) mean that "fast" wind from coronal holes (Zirker, 1977) can be reduced to low speeds in near-Earth space, while "slow" wind from the streamer belt (Crooker *et al.*, 1996; Eselevich, Fainshtein, and Rudenko, 1999) can be accelerated to relatively high speeds by 1 AU. This makes the interpretation of solar wind observations in terms of coronal processes somewhat complex, particularly in the ecliptic plane, as stream interactions are maximised at low heliographic latitudes (McComas *et al.*, 2003; Owens and Forsyth, 2013).

Conversely, there are properties of the solar wind that are relatively unaffected by in-transit effects and hence are fixed by processes in the corona. As the solar wind plasma is highly electrically conducting, the plasma and HMF are effectively frozen together (Priest, 1982) and different plasma regimes can't efficiently mix. This means the elemental composition of the solar wind does not change significantly from its source value, except on small scales as a result of heliospheric magnetic reconnection (Gosling *et al.*, 2007) or differential ion streaming along the HMF direction (Yohei *et al.*, 2004). The solar wind is also collisionless, thus ion charge states cannot evolve through recombination of ions and electrons. As a result, charge states of the heavier solar wind elements (which are not fully ionised) provide information about the electron temperature back in the corona, where the plasma was last collisional (Owocki, Holzer, and Hundhausen, 1983). Quantitative interpretation of these signatures is not straightforward as coronal electron density, temperature and plasma velocities all influence the ultimate ion charge states (Landi *et al.*, 2012; Zhao *et al.*, 2014). But in general higher ion charge states in the solar wind are indicative of hotter coronal source regions.

Compositional and heavy ion charge-state measurements have been shown to be a reliable indicator of the boundaries between different solar wind types, even when solar wind properties, particularly solar wind speed, have been significantly altered by stream interaction processes (Geiss, Gloeckler, and von Steiger, 1995; von Steiger *et al.*, 2000). Slow solar wind is associated with hotter coronal regions and significantly enhanced abundance of low first-ionisation potential (FIP) elements relative to the photosphere, while fast wind is from cooler coronal-hole regions, with elemental composition closer to that of the photosphere. Heavy ion properties have also been used to both identify (Lepri *et al.*, 2001) and diagnose ICMEs (Zurbuchen *et al.*, 2003). ICMEs typically have heavy ion properties consistent with hot coronal source regions, elevated above even the slow solar wind (Lepri and Zurbuchen,

2004). However, rare ICMEs with low ion charge states (Gloeckler *et al.*, 1999), attributed to filamentary material (Song *et al.*, 2017), and coronal-hole-like composition (Gosling *et al.*, 1998), have also been observed. This high event-to-event variability within heavy ion signatures of ICMEs (Song *et al.*, 2016), means it can be difficult to identify common patterns and classes of event which can help determine coronal formation/release processes.

In this study we take a statistical approach to the properties and variations in composition and ion charge-state signatures within ICMEs. In Section 3, we first present a comparison between magnetic clouds and non-cloud ICMEs. In Section 4, events are further divided into fast and slow magnetic cloud and non-cloud ICMEs. In Section 5, we summarise the key findings and discuss the implications for CME formation and acceleration.

2. Data

Solar wind composition and ion charge-state information are provided by the *Advanced Composition Explorer* (ACE) *Solar Wind Ion Composition Spectrometer* (SWICS) instrument (Gloeckler *et al.*, 1998). We use the 1-h "merged" dataset (available at ftp://cdaweb. gsfc.nasa.gov/pub/data/ace/multi), which also contains ACE solar wind magnetic field and plasma data (McComas *et al.*, 1998; Smith *et al.*, 1998) at the same 1-h resolution. Data are available for 1998 to June 2011. In principle, higher resolution charge-state information is possible with the SWICS instrument, but this at the limit of the instrument sensitivity and thus requires bespoke processing, meaning its use is generally limited to case studies (Kepko *et al.*, 2016), rather than the long-term statistical analyses presented here.

Interplanetary coronal mass ejection timings and classifications are taken from the updated Cane and Richardson (2003) ICME catalogue, available from http://www.srl.caltech. edu/ACE/ASC/DATA/level3/icmetable2.htm. In addition to magnetic cloud and non-cloud ICME types, the Cane and Richardson (2003) catalogue includes a third, "cloud-like ICME", classification. Such ICMEs generally show variations in both solar wind and compositional parameters intermediate between magnetic cloud and non-cloud ICMEs and thus are omitted from the rest of the study for clarity. This leaves 97 magnetic clouds and 118 non-cloud ICMEs in the available dataset, which are considered in the remainder of this study.

3. Magnetic Cloud and Non-cloud ICMEs

We first consider the duration of ICMEs and their sheath regions. The top-left panel of Figure 1 shows that the distributions of ICME durations for magnetic cloud and non-cloud ICMEs are similar. Applying a Kolmogorov–Smirnov non-parametric test to the null hypothesis (that the distributions of magnetic cloud and non-cloud ICME durations are merely subsamples of the same underlying distribution), a statistically significant difference is not present at the 95% confidence level. In both cases, the average duration is approximately 1 day, but with a long tail to the distribution, giving a median duration of 1.25 days. The top-right panel shows that the distributions of ICME sheath durations (strictly speaking this is the upstream disturbance duration, as not all ICMEs drive heliospheric shocks) also appear very similar for magnetic cloud and non-cloud ICMEs. Again, using the Kolmogorov–Smirnov test, there is no statistically significant difference between the distributions. The median (mean) sheath duration is 0.25 (0.31) days.

In order to consider the solar wind context of ICMEs, Figure 2 shows the ICME occurrence as a function of solar cycle. The occurrence time of each ICME is converted to solar
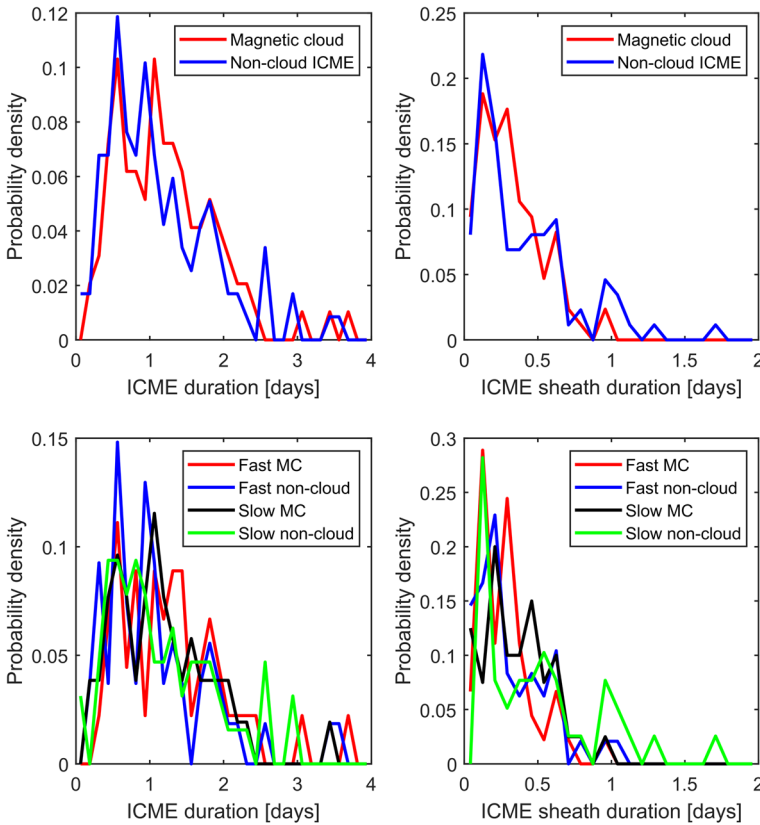
Figure 1 Probability density functions for (*left*) ICME durations and (*right*) the duration of the upstream disturbance, typically referred to as the ICME sheath when the disturbance is a heliospheric shock. *Top panels* show ICMEs split into magnetic clouds (*red*) and non-cloud ICMEs (*blue*). *Bottom panels* show further division by average ICME speed observed *in situ*, using a threshold of 450 km s^{-1}. This results in fast magnetic clouds (*red*), slow magnetic clouds (*black*), fast non-cloud ICMEs (*blue*) and slow non-cloud ICMEs (*green*).

cycle phase, which runs from 0 to 1 from solar minimum to solar minimum, assuming Solar Cycle 24 has a length of 10 years (Owens *et al.*, 2011). Given the dataset spans two incomplete solar cycles, there is a systematic observing bias in occurrence, but this bias is the same for all ICME types. Thus we can still conclude that there is no difference in the solar cycle occurrence of magnetic clouds with respect to non-cloud ICMEs.

We next consider the ICME average properties. Solar wind and heavy ion properties are averaged over the whole ICME duration and the resulting distributions compared. An example is shown in Figure 3 for the average magnetic field intensity, $|\mathbf{B}|$, in non-cloud (blue) and magnetic cloud (red) ICMEs. The probability density function (PDF) is shown in the left-hand panel, with data sorted into 0.5 nT bins. Due to the relatively low number of events (118 non-cloud ICMEs and 97 magnetic cloud ICMEs), the PDFs are highly discretised. While we can (and do) perform statistical tests, it can be difficult to easily see if distributions really differ and, more importantly, this conclusion may change with the (arbitrary) choice of bin size. For this reason, the cumulative distribution functions (CDFs) shown in the middle panel are preferable, as bin size is irrelevant. The CDFs can be made more intu-
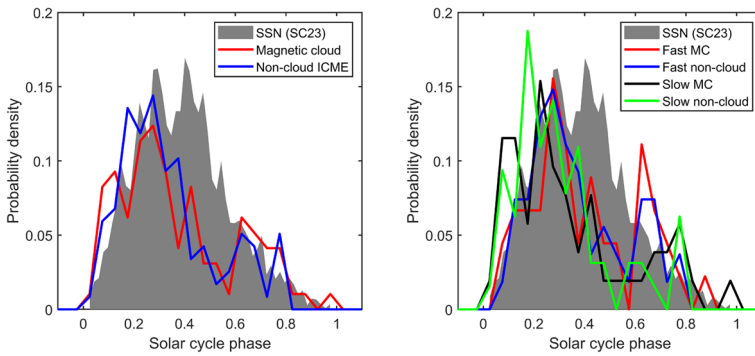
Figure 2 Occurrence of difference ICME types with solar cycle phase, defined as 0 at the solar minimum at the start of the cycle and 1 at the solar minimum at the end of the cycle. The *grey-shaded area* shows the sunspot number for Solar Cycle 23, with the amplitude arbitrarily scaled. *Left*: Magnetic cloud (*red*) and non-cloud (*blue*) ICMEs. *Right*: ICMEs further divided into fast magnetic clouds (*red*), slow magnetic clouds (*black*), fast non-cloud ICMEs (*blue*) and slow non-cloud ICMEs (*green*).
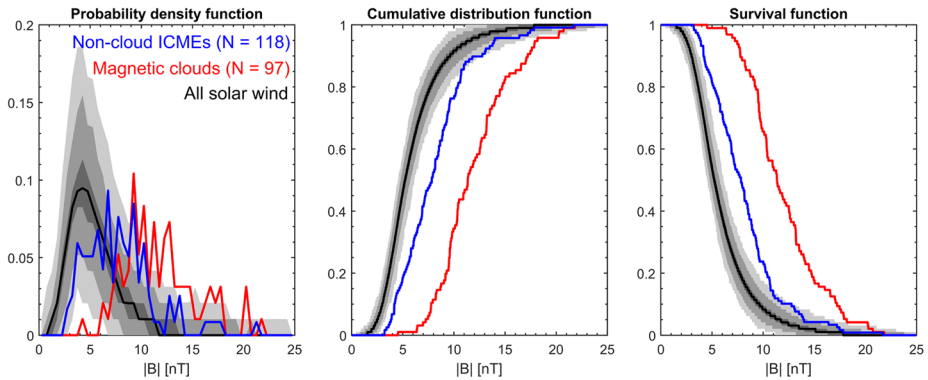

Figure 3 Average magnetic field intensity, |B|, in non-cloud ICMEs (*blue*), magnetic clouds (*red*) and ambient solar wind (*black*). *Grey shaded areas* show the 1-, 2- and 3-sigma intervals from Monte Carlo sampling of the solar wind. *Left*: The probability density functions (PDFs) using 0.5 nT bins. *Middle*: The cumulative distribution functions (CDFs). *Right*: The survival function, 1-CDF, which shows the probability of exceeding a given |B| threshold.

itive to interpret if displayed as a 1-CDF, often called the complementary CDF or "survival function", shown in the right-hand panel. The survival function equates to the fraction of ICMEs which exceed a given |B| value. For example, 24% of non-cloud ICMEs have an average |B| greater than 10 nT, whereas it is 66% for magnetic clouds.

Also shown in Figure 3 are the PDF, CDF and survival function of |B| for the solar wind as a whole. In order to quantify sampling error in the ICME distributions, the solar wind sample uses the same sample size as ICMEs. A Monte Carlo approach is used: 97 days of solar wind data from the 1998 and 2012 interval (with ICMEs removed) are randomly selected, daily mean values computed and the PDF constructed. This random sampling is performed 1000 times, which was found to produce a convergent solution. 1-day intervals are used as this is a typical ICME duration, whereas 97 samples was chosen as this is the smallest sample size used for the ICME categories and thus represents the upper limit of the sampling uncertainty. The black line shows the median of the 1000 samples, the grey-

shaded areas show the 1-, 2- and 3-sigma intervals. The survival function (right-hand panel) shows two important features. Firstly, both magnetic cloud and non-cloud ICMEs have significantly elevated $|\boldsymbol{B}|$ properties compared to the solar wind as whole. This is true above the 3-sigma (99.7%) confidence level. Secondly, the difference between the non-cloud and magnetic cloud ICMEs is unlikely to be the result of limited sample size: for $N = 97$ at a probability of 0.5, the 3-sigma sampling uncertainty in $|\boldsymbol{B}|$ for all solar wind is approximately ± 1 nT, whereas the difference between non-cloud and magnetic cloud ICMEs is approximately 4 nT. This is confirmed by the non-parametric Kolmogorov–Smirnov test, which rejects at the 99.9% confidence level the null hypothesis (that the magnetic cloud and non-cloud $|\boldsymbol{B}|$ distributions are subsamples of the same underlying distribution). Given that enhanced $|\boldsymbol{B}|$ is part of the definition by which magnetic clouds are identified (Burlaga, 1988; Cane and Richardson, 2003), this is not surprising and could be largely a selection effect.

Figure 4 shows survival functions for all the *in situ* parameters considered in this study. Above each plot is the Kolmogorov–Smirnov significance level at which non-cloud and magnetic cloud ICMEs can be said to be statistically different. As shown in Figure 3, the average magnetic field intensity is elevated in magnetic clouds relative to non-cloud ICMEs. Conversely, magnetic cloud and non-cloud ICMEs are indistinguishable from each other in terms of their average plasma properties, namely radial proton speed (V_X), density (n_p) and temperature (T_p). Both magnetic cloud and non-cloud ICMEs, however, have elevated n_p and reduced T_p relative to the ambient solar wind. Again, there may be event selection bias at play here, as reduced proton temperature is one of the key signatures used to identify ICMEs (Cane and Richardson, 2003).

Ion composition measures, namely the alpha-to-proton and iron-to-oxygen (Fe:O) number ratios, are significantly different between ICME types, with magnetic clouds showing elevated values in both cases. Both cloud and non-cloud ICMEs show elevated abundances of heavy ions with respect to the ambient solar wind, as has been previously reported (Borrini *et al.*, 1983; Zurbuchen *et al.*, 2003). The O^{7+}:O^{6+} ratio and average charge state of oxygen ($\langle q_O \rangle$) are also significantly enhanced in magnetic clouds relative to non-cloud ICMEs (Henke *et al.*, 1998). Conversely, average C and Fe charge states show no statistically significant difference between magnetic clouds and non-cloud ICMEs (though Fe charge states are higher for magnetic clouds than non-cloud ICMEs, particularly in the tail of the distribution. This is also seen in Figure 5, discussed below). However, ICME Fe charge states are highly elevated relative to the ambient solar wind, as expected (Lepri *et al.*, 2001; Lepri and Zurbuchen, 2004).

In order to gain a more complete picture of ICME properties, we now consider the ICME time profiles, rather than just average properties. The times of the ICME leading and trailing edges at ACE are here denoted t_{LE} and t_{TE}, respectively. Figure 5 shows a "double composite", also known as a super-posed epoch or Chree analysis (Chree and Stagg, 1928), of ICMEs using both t_{LE} and t_{TE} as reference times, with the duration of each ICME normalised to 1 day. One day prior to t_{LE} and following t_{TE} is also shown in Figure 5. For fast ICMEs driving interplanetary shocks, the $t_{LE} - 1$ to t_{TE} interval will contain the ICME sheath region, as Figure 1 shows the typical duration is ≈ 0.2 days. Red lines and pink shaded regions in Figure 5 show median and 1-sigma variations for magnetic clouds, while blue lines and blue shaded regions show the same for non-cloud ICMEs.

Average plasma properties, V_X, n_p and T_p, are shown by panels b, c and d of Figure 5, respectively. Within the body (*i.e.* $t_{LE} < t < t_{TE}$) of magnetic cloud and non-cloud ICMEs, these properties are very similar, *i.e.*, the median values agree to within the 1-sigma error bands. Both magnetic cloud and non-cloud ICMEs show signatures of quasi-adiabatic expansion, with reduced n_p (panel c) and T_p (panel d) relative to the upstream solar wind, as well as a declining V_X profile (panel b) through the ICME itself.
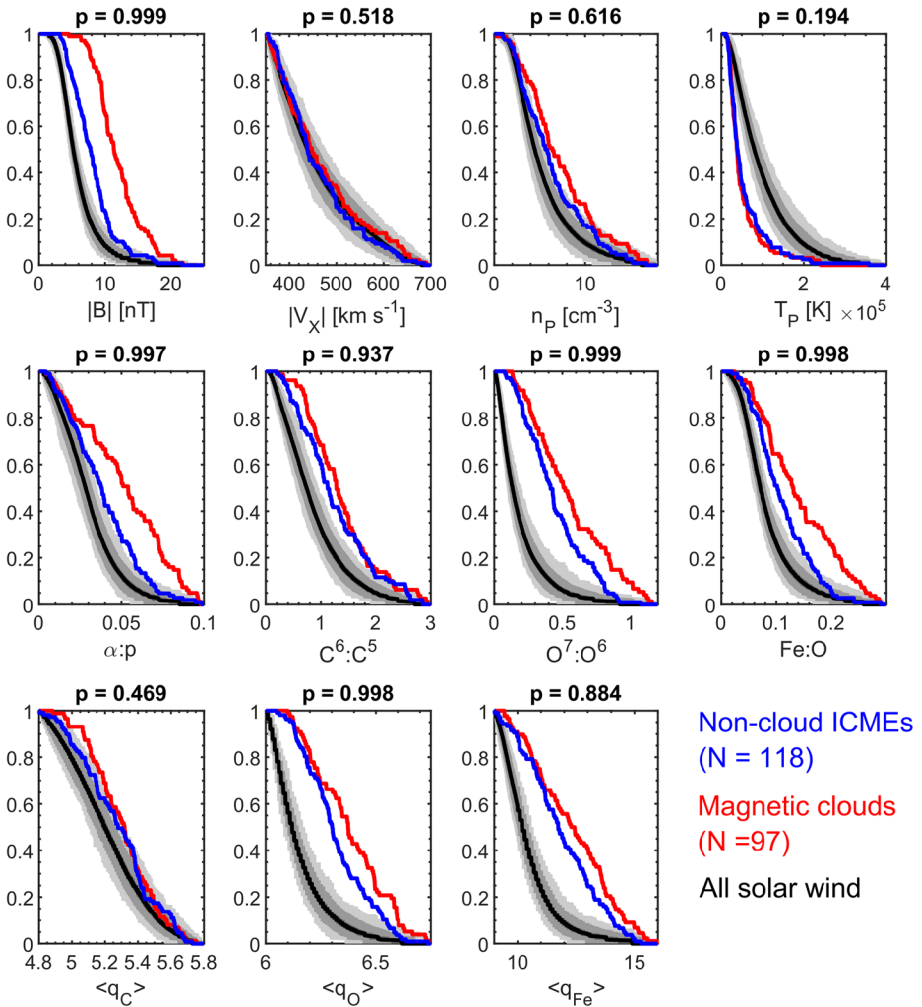
Figure 4 Survival functions for non-cloud ICMEs (*blue*), magnetic clouds (*red*) and ambient solar wind (*black*), in the same format as Figure 3. Parameters considered are average magnetic field intensity ($|\mathbf{B}|$), proton speed ($|V_X|$), proton density (n_p), proton temperature (T_p), the alpha-to-proton number ratio (α:p), carbon (C^{6+}:C^{5+}) and oxygen (O^{7+}:O^{6+}) charge-state ratios, the iron-to-oxygen ion number ratio (Fe:O) and the average charge states of carbon ($\langle q_C \rangle$), oxygen ($\langle q_O \rangle$) and iron ($\langle q_{Fe} \rangle$). Above each plot is the statistical significance of the difference between the non-cloud and magnetic cloud ICMEs.

Immediately ahead of both cloud and non-cloud ICME leading edge (*i.e.* $t_{LE} - 0.5 < t < t_{LE}$), the sheath of compressed solar wind takes the form of enhanced $|\mathbf{B}|$ (panel a), V_X (panel b), n_p (panel c) and T_p (panel d). The enhancements of $|\mathbf{B}|$ and n_p are greater for magnetic clouds than non-cloud ICMEs, suggesting stronger compression despite the similar speed profiles within ICME types. This signature is consistent with magnetic clouds resulting from ICME encounters close to the centre of an ICME, with non-cloud ICMEs resulting from "glancing blows." We also note, however, that the enhanced compression ahead of magnetic clouds could also partly be the result of the systematically slower speeds observed in the uncompressed solar wind upstream of magnetic clouds (*i.e.* $t_{LE} - 1 < t <$
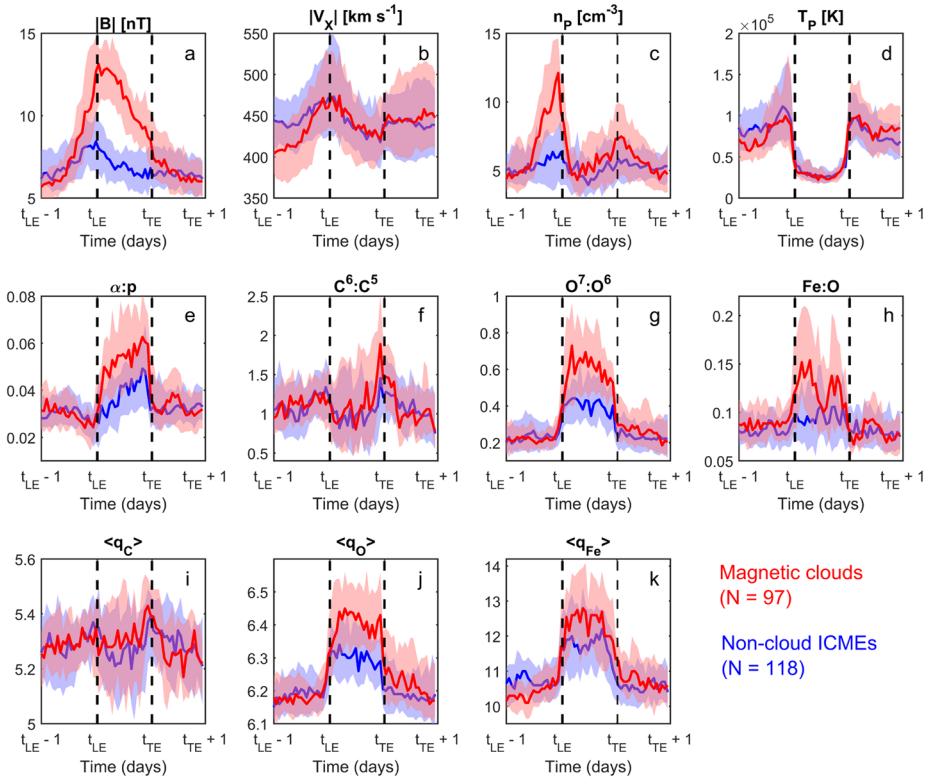
Figure 5 A composite analysis of ICMEs observed by ACE between 1998 and 2012. Composite time are ICME leading (t_{LE}) and trailing (t_{TE}) edges, shown as vertical dashed lines. The duration of each ICME, *i.e.* $t_{TE} - t_{LE}$, has been normalised to 1 day. The composite window spans a further 1 day prior to t_{LE}, and 1 day following t_{TE}. *Red* and *blue lines* show the median values for magnetic clouds and non-cloud ICMEs, respectively. Shaded areas show the 1-sigma range. Panels show: (**a**) magnetic field intensity, (**b**) proton speed, (**c**) proton density, (**d**) proton temperature, (**e**) alpha-to-proton ratio, (**f**) C^{6+}-to-C^{5+} ratio, (**g**) O^{7+}-to-O^{6+} ratio, (**h**) Fe-to-O ratio, (**i**) average charge state of C, (**j**) average charge state of O and (**k**) average charge state of Fe.

$t_{LE} - 0.5$) compared to that for non-cloud ICMEs. As previously noted, $|\boldsymbol{B}|$ within the body of magnetic clouds is significantly enhanced relative to non-cloud ICMEs (panel a). Though this is at least partly a selection effect, it is, however, still consistent with magnetic cloud encounters being closer to the centre of an ICME than non-cloud events, with a fall-off in $|\boldsymbol{B}|$ expected with distance from the centre of a magnetic flux rope (Lepping, Jones, and Burlaga, 1990).

We now consider the compositional and ion charge-state properties. As expected, the sheath regions ahead of ICMEs show heavy ion properties characteristic of the ambient solar wind, rather than the body of the ICMEs. There is a weak decline in the O^{7+} to O^{6+} ratio through the body of magnetic clouds, though it is less apparent in $\langle q_O \rangle$. The enhancement in $\langle q_O \rangle$ for magnetic clouds relative to non-cloud ICMEs is greater than the equivalent for $\langle q_{Fe} \rangle$. This suggests any preferential heating of magnetic cloud plasma occurs primarily in the low corona. The C^{6+} to C^{5+} ratio (and $\langle q_C \rangle$) shows little overall enhancement within either magnetic cloud or non-cloud ICMEs. Carbon charge-state profiles, however, do show

an interesting feature: there is an enhancement at (and just behind) the trailing edge of magnetic clouds.

The alpha-to-proton ratio shows a gradual increase from the leading to trailing edge of both magnetic clouds and non-cloud ICMEs. Conversely, there is a suggestion of a decline, or possibly double peaked variation, in Fe:O through the body of magnetic clouds, and a reduction immediately behind magnetic clouds. Note, however, that the uncertainty bands are large due to high event-to-event variability.

In the uncompressed ambient solar wind ahead of ICME sheath regions (*i.e.* the interval $t_{LE} - 1 < t < t_{LE} - 0.5$), $\langle q_{Fe} \rangle$ is slightly higher for non-clouds than for magnetic clouds. This is somewhat at odds with the reduced V_X ahead of magnetic clouds, as the slow solar wind is typically associated with hotter coronal source regions than the fast wind (Gloeckler, Zurbuchen, and Geiss, 2003; von Steiger *et al.*, 2000).

4. Fast and Slow ICMEs

We now further stratify the dataset by average ICME speed. A threshold of 450 km s^{-1} is used as it approximately bisects both magnetic clouds and non-cloud ICME distributions. The bottom-left panel of Figure 1 shows ICME duration for the four different ICME types. A Kolmogorov–Smirnov test reveals no statistically significant differences in ICME durations. For ICME sheath durations, shown in the bottom-right panel of Figure 1, the distributions appear similar by eye. But statistical testing suggests the sheath durations ahead of fast magnetic clouds are distinct from both slow magnetic clouds and slow non-cloud ICMEs, while the durations of sheaths ahead of fast non-cloud ICMEs are statistically distinct from those ahead of slow non-cloud ICMEs. The right-hand panel of Figure 2 shows that fast ICMEs, both magnetic cloud and non-cloud, are more prevalent during the declining phase than their slower counterparts. This could potentially lead to a systematic difference in the ambient solar wind encountered by fast ICMEs compared to slow ICMEs.

Figure 6 and Figure 7 show survival functions for solar wind and heavy ion properties, respectively, of the four ICME types and averaged over different ICME regions; the ICME body, the ICME sheath and the upstream/downstream ambient solar wind. Red indicates a survival function of 1 (*i.e.* all ICMEs are above a given value), white indicates 0.5 (*i.e.* the median value) and blue indicates 0 (*i.e.* no ICMEs have this value).

We first consider the average properties within the ICME body. These properties are also summarised in Table 1 in terms of the statistical significance of differences between ICME types. Specifically, numbers show the *p*-value at which we can reject the null hypothesis that average properties of two ICME types are subsamples of the same underlying distribution (*i.e.* they are statistically indistinguishable). Values have been colour-coded such that blue (red) values correspond to ICME properties that can be considered to be significantly different (the same). We here highlight a few points of note:

– Fast magnetic clouds are indistinguishable from slow magnetic clouds in terms of average $|\boldsymbol{B}|$, but are distinct in terms of plasma properties, with fast magnetic clouds showing higher V_X (by definition), lower n_p and higher T_p.

– Fast magnetic clouds have elevated $|\boldsymbol{B}|$ values compared to fast non-cloud ICMEs, but indistinguishable plasma properties.

– There are no significant differences in $\langle q_C \rangle$ between any of the four ICME types. (But the $C^{6+}:C^{5+}$ ratio is significantly different between fast magnetic clouds and slow non-cloud ICMEs.)
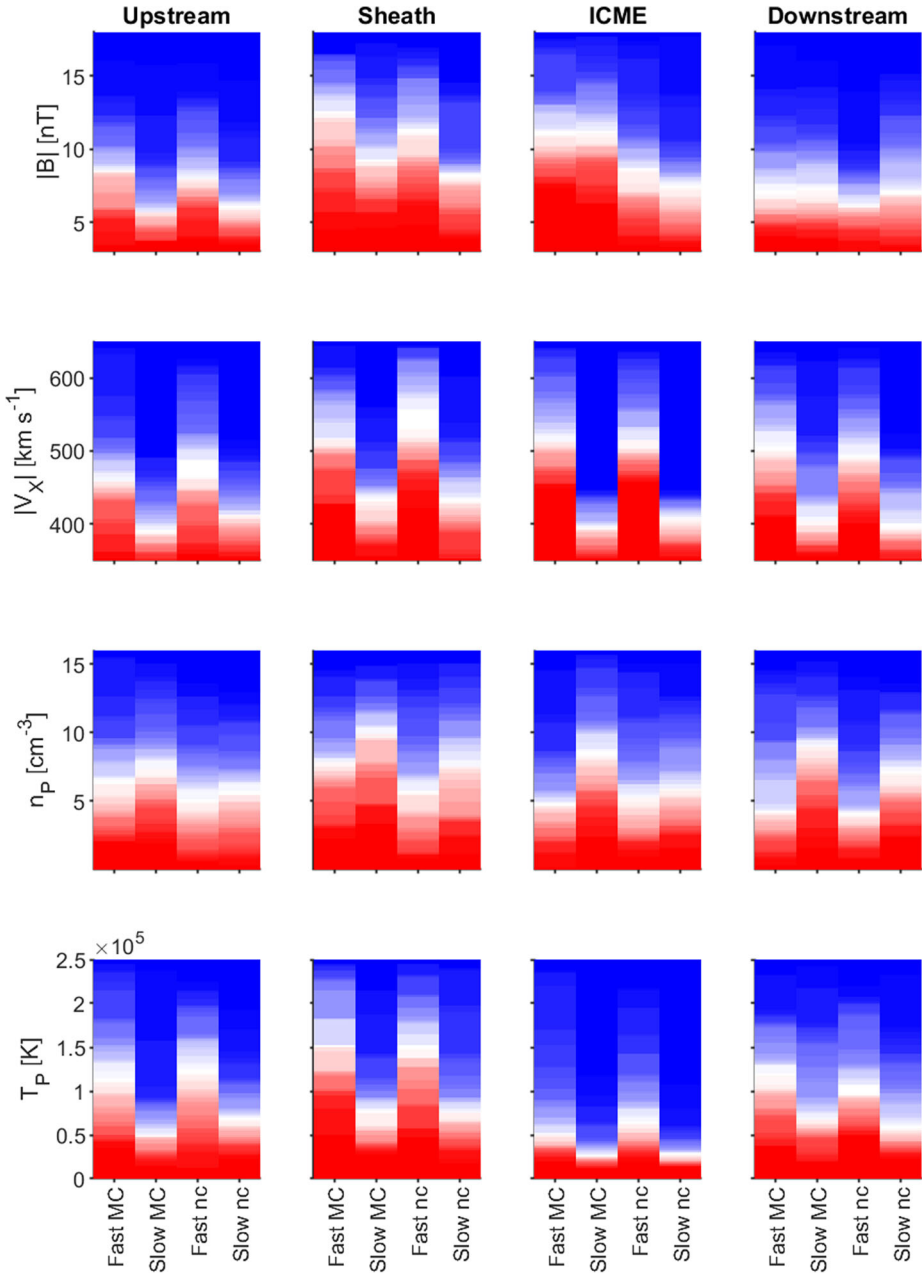
Figure 6 Survival functions for solar wind properties of different ICME types and within different ICME regions. Red indicates a survival function of 1 (*i.e.* all ICMEs are above a given value), white indicates 0.5 (*i.e.*, the median value) and blue indicates 0 (*i.e.* no ICMEs have this value). Each panel shows, from left to right: Fast magnetic cloud (MC), slow MC, fast non-cloud (nc), and slow nc ICMEs. *Columns of panels*, from left to right show the 0.5-day solar wind interval upstream of the ICME sheath, the ICME sheath, the ICME body and the 0.5-day solar wind interval downstream of the ICME trailing edge.
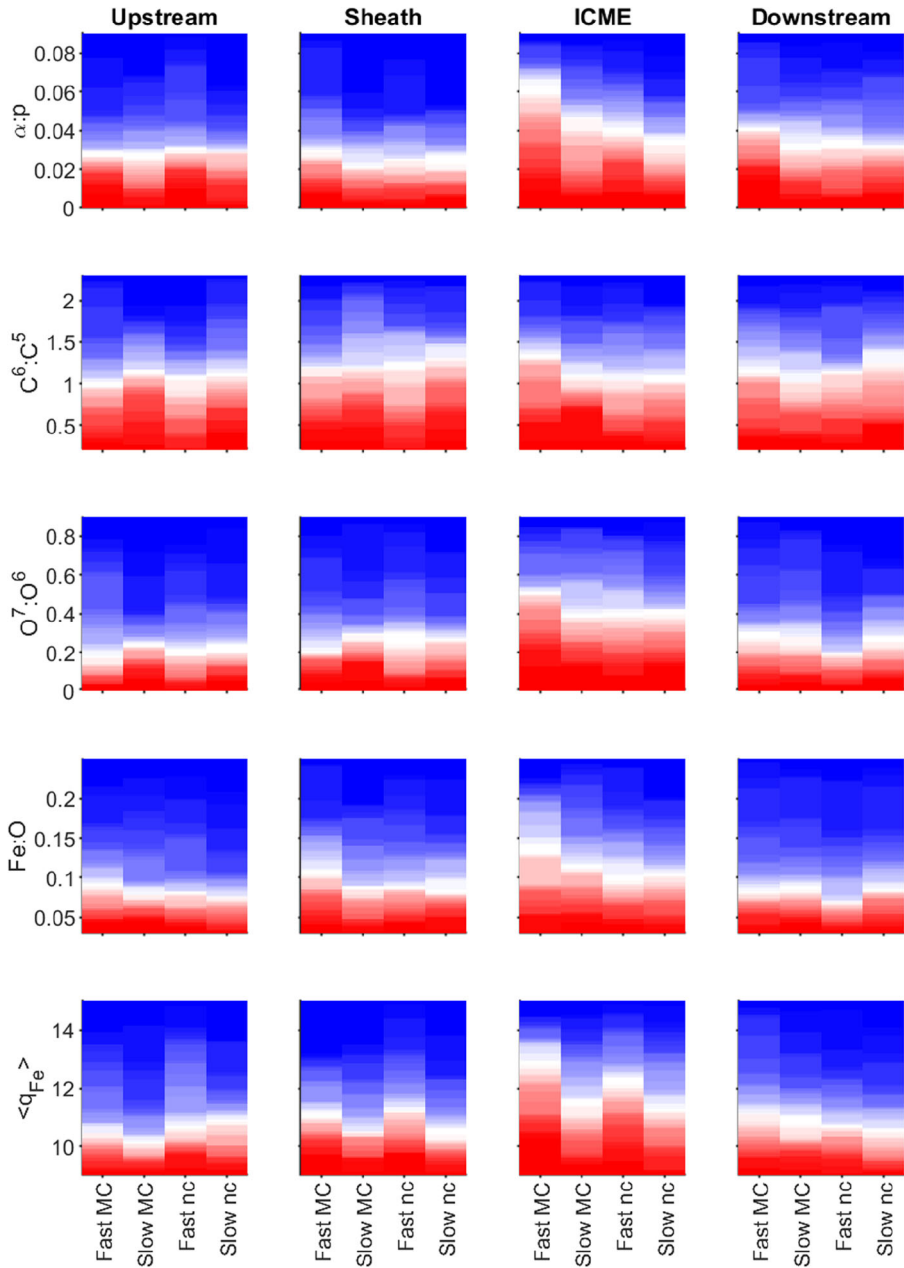
Figure 7 The same as Figure 6, but for heavy ion charge-state and composition parameters.

– Fast magnetic clouds exhibit significantly elevated O and Fe charge states compared to all other ICME types.

– Fast non-cloud ICMEs exhibit elevated Fe charge states compared with slow magnetic cloud and non-cloud ICMEs, but the O charge states are indistinguishable.

Table 1 A comparison of average properties in different ICME types. Numbers show the p-value at which the null hypothesis (that average properties of two ICME types are subsamples of the same underlying distribution) can be rejected. Values have been colour-coded so that $p < 0.9$ is *red*, while $p > 0.95$ is *blue*. Intermediate values are *white*. Thus *blue* (*red*) values correspond to ICME properties that can be considered to be significantly different (the same).

	Plasma				Ion charge-states					Composition	
	$\|B\|$	$\|V_X\|$	n_p	T_p	$C^6{:}C^5$	$O^7{:}O^6$	$<q_C>$	$<q_O>$	$<q_{Fe}>$	Fe:O	α:p
Fast MC (N=45)											
... slow MC	0.35	0.99	0.99	0.99	0.85	0.97	0.62	0.99	0.99	0.87	0.99
... fast non-cloud	0.99	0.01	0.35	0.42	0.95	0.99	0.52	0.99	0.98	0.99	0.99
... slow non-cloud	0.99	0.99	0.97	0.99	0.99	0.99	0.23	0.99	0.99	0.99	0.99
Slow MC (N=52)											
... fast MC	0.35	0.99	0.99	0.99	0.85	0.97	0.62	0.99	0.99	0.87	0.99
... fast non-cloud	0.99	0.99	0.99	0.99	0.81	0.90	0.40	0.07	0.93	0.69	0.47
... slow non-cloud	0.99	0.87	0.96	0.16	0.55	0.93	0.37	0.74	0.02	0.61	0.71
Fast non-cloud (N=54)											
... fast MC	0.99	0.01	0.35	0.42	0.95	0.99	0.52	0.99	0.98	0.99	0.99
... slow MC	0.99	0.99	0.99	0.99	0.81	0.90	0.40	0.07	0.93	0.69	0.47
... slow non-cloud	0.96	0.99	0.79	0.99	0.47	0.08	0.11	0.64	0.94	0.10	0.94
Slow non-cloud (N=64)											
... fast MC	0.99	0.99	0.97	0.99	0.99	0.99	0.23	0.99	0.99	0.99	0.99
... slow MC	0.99	0.87	0.96	0.16	0.55	0.93	0.37	0.74	0.02	0.61	0.71
... fast non-cloud	0.96	0.99	0.79	0.99	0.47	0.08	0.11	0.64	0.94	0.10	0.94

– Slow magnetic clouds and slow non-cloud ICMEs are indistinguishable in terms of composition or ion charge states, with the possible exception of $O^{7+}{:}O^{6+}$.
– Fast magnetic clouds display elevated alpha-to-proton occurrence relevant to all other ICME types. Fe:O is also elevated compared to non-cloud ICMEs, with only a minor enhancement relative to slow magnetic clouds.
– Slow magnetic clouds, fast non-clouds and slow non-clouds are indistinguishable in terms of composition.

We next consider the other three ICME regions: the ICME sheath, and the upstream/downstream ambient solar wind:

– As expected by compression due to relative motion, the sheath regions ahead of fast ICMEs (both magnetic cloud and non-cloud) show enhanced $|B|$ and $|V_X|$ in comparison with slow ICMEs (both magnetic cloud and non-clouds).
– Fast ICMEs (both magnetic cloud and non-cloud) are embedded (both up and down stream) in faster, less dense and hotter ambient solar wind than slow ICMEs.
– The ambient solar wind upstream of fast ICMEs has elevated Fe charge states, but reduced O and C charge states compared with that for slow ICMEs.

Finally, we consider the time profiles for fast and slow ICMEs. The median properties are shown in Figure 8. Uncertainty bands are omitted for clarity.

While fast and slow magnetic clouds show approximately equal average $|B|$ within the ICME body, the time profiles are very different. Slow clouds show an approximately "domed" $|B|$ profile, roughly symmetric about the ICME mid-point. This is close to that expected of a spacecraft trajectory through a quasi-force-free magnetic flux rope (Burlaga *et al.*, 1981; Owens, Merkin, and Riley, 2006; Riley *et al.*, 2004). Fast magnetic clouds instead show a sharp decline in $|B|$ from the leading edge to the trailing edge, suggesting significant compression at the front of fast magnetic clouds due to interaction with the (slower) upstream solar wind. Both fast and slow non-cloud ICMEs show little $|B|$ enhancement
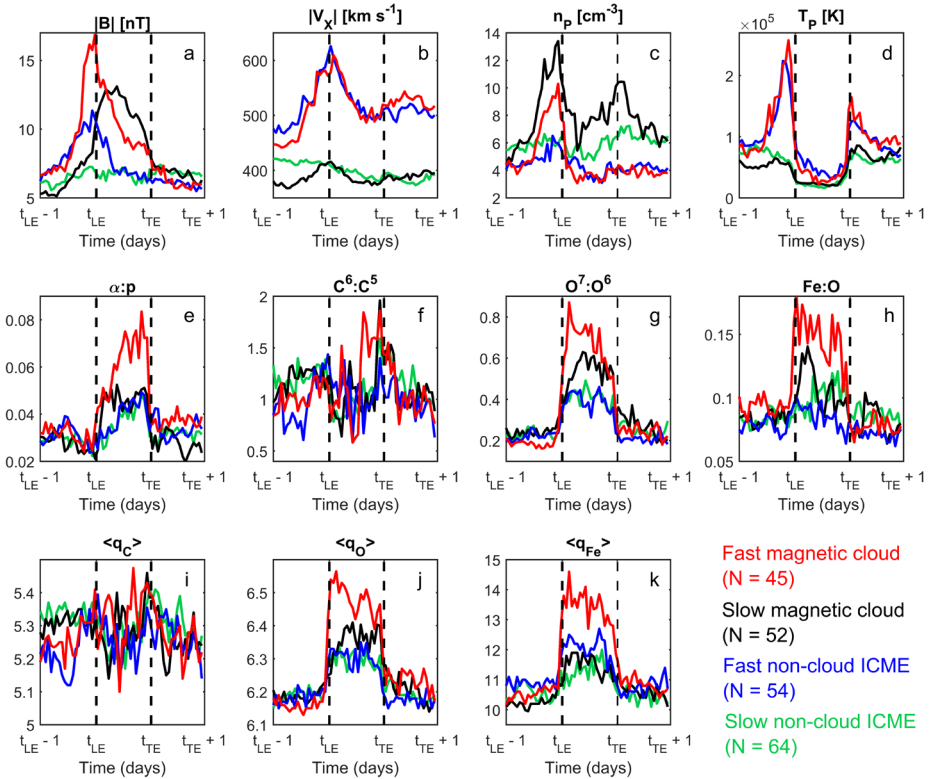
Figure 8 The same as Figure 5, but separating fast (*red*) and slow (*black*) magnetic clouds, and fast (*blue*) and slow (*green*) non-cloud ICMEs, using a threshold of $450 \, \text{km s}^{-1}$ for the average speed inside the ICME. Error bars are not shown for clarity.

above the ambient solar wind level. Fast non-cloud ICMEs, however, do show an enhancement in $|\boldsymbol{B}|$ just behind the ICME leading edge, likely due to compression resulting from interaction with the slower upstream solar wind.

In contrast to the $|\boldsymbol{B}|$ profile, there is little difference in the speed profiles of fast magnetic clouds and fast non-cloud ICMEs (or between slow magnetic clouds and slow non-cloud ICMEs). Both types of fast ICME show a strongly declining speed profile within the ICME, indicating continued expansion at 1 AU. Ambient solar wind speed is enhanced immediately ahead of fast ICMEs, as a result of the compressed sheath region. This is also seen in the increased n_p and T_p in the ambient solar wind ahead of fast ICMEs. The n_p enhancement is stronger for fast magnetic clouds than for fast non-cloud ICMEs. The interiors of slow ICMEs show weakly declining speed profiles, suggesting some continued expansion at 1 AU. The decreased T_p, however, suggests all ICMEs undergo significant radial expansion at some point between the corona and 1 AU, regardless of 1-AU speed. We note that as a decreased T_p is one of the signatures used to identify ICMEs in *in situ* data (Cane and Richardson, 2003), this could be partly due to selection.

Looking at the ion charge-state and compositional time profiles, fast magnetic clouds again appear distinct from both slow magnetic clouds and fast/slow non-cloud ICMEs. This is most apparent in the alpha-to-proton ratio, where fast magnetic clouds show a rising profile to a peak value of around 8%, whereas slow magnetic clouds and non-cloud ICMEs

show more of a flat profile with values of around $4-5\%$ (which is still elevated above the ambient solar wind value of around $2-3\%$). Similarly, Fe:O is significantly higher for fast magnetic clouds, though here slow magnetic clouds also show somewhat elevated values relative to non-cloud ICMEs, particularly near the ICME leading edge. In O and Fe charge states, fast magnetic clouds exhibit the highest values, with slow magnetic clouds taking intermediate values for O, but exhibiting similar values to non-cloud ICMEs for Fe. C charge states are similar to the ambient solar wind, except for an enhancement near the rear of fast magnetic clouds, and, for a shorter duration, slow magnetic clouds.

5. Discussion and Conclusions

Solar wind and heavy ion measurements within interplanetary coronal mass ejections (ICMEs) are able to potentially provide insight into the formation and evolution of ejecta. This study has provided a comprehensive statistical analysis of approximately 200 ICMEs observed by the ACE spacecraft between January 1998 and June 2011.

In terms of solar wind properties, magnetic clouds show highly elevated magnetic field intensities relative to non-cloud ICMEs, though this may be at least partly a selection effect. Plasma parameters within magnetic cloud and non-cloud ICMEs are indistinguishable, with both showing evidence of increased expansion and quasi-adiabatic cooling relative to the ambient solar wind. Despite the similar internal speed profiles in magnetic cloud and non-cloud ICMEs, magnetic clouds show significantly stronger compression of the upstream ambient solar wind in the ICME sheath. As compression is expected to peak at the nose of the ICME (Owens *et al.*, 2005; Russell and Mulligan, 2002), this could be interpreted as non-cloud ICMEs being glancing blows, *i.e.* the spacecraft encounters a flux rope further from the flux-rope central axis. However, this scenario would also result in non-cloud ICMEs having thicker sheath regions than magnetic clouds (Owens and Cargill, 2004; Russell and Mulligan, 2002), which is not observed. We also note that the solar wind upstream of magnetic clouds is generally slower than non-cloud ICMEs, consistent with magnetic clouds occurring as bubbles along the channel of slowest solar wind associated with the heliospheric current sheet (Crooker *et al.*, 1990). In this case the additional compression in magnetic cloud sheath regions could simply be the result of increased ICME speed in the ambient solar wind frame of reference.

While both magnetic cloud and non-cloud ICMEs generally show enhanced heavy ion abundance and charge states compared to the ambient solar wind, magnetic clouds are generally further elevated above non-cloud ICMEs. This is true for the alpha-to-proton and Fe:O abundance ratios, as well as O and Fe charge states. C charge states within both types of ICME are comparable to the ambient solar wind, except at the trailing edge of ICMEs, where they are enhanced. The interpretation of charge-state data is complex, as coronal electron density, temperature and plasma velocities all play a role in determining the ionisation and recombination rates (Landi *et al.*, 2012; Zhao *et al.*, 2014). Coronal mass ejections may significantly disrupt ambient coronal structure, further complicating interpretation of charge-state data (Boe *et al.*, 2018; Ding and Habbal, 2017). Thus, ideally, self-consistent dynamical modelling (Shen *et al.*, 2017) should be used to enable interpretation of *in situ* heavy ion observations in terms of coronal processes. But there are some broad trends that can be exploited to enable a preliminary interpretation. Recently, it has been suggested that Fe charge states are generally enhanced by continual heating in an extended range of coronal heights, whereas C and O charge states are more greatly affected by heating in the lower corona (Gruesbeck *et al.*, 2011;

Lepri *et al.*, 2012; Song *et al.*, 2016). Thus magnetic clouds could be more greatly associated with flare heating in the low corona (Lepri and Zurbuchen, 2004) than non-cloud ICMEs. This could result from either intrinsically different formation and acceleration mechanisms between two different types of eruption, or due to spatial variation and spacecraft sampling within a single type of CME. There is evidence in O and Fe charge states of a declining coronal source temperature through magnetic clouds. This may be the result of a reduction in flare-related heating through the lifetime of the magnetic flux-rope formation.

While ICMEs are routinely classified as either magnetic cloud or non-cloud events, we also found it instructive to further divide these two classes into fast and slow events. Slow magnetic clouds are not found to be weaker than fast magnetic clouds in terms of magnetic field intensity within the ICME body (Gonzalez *et al.*, 1998; Owens and Cargill, 2002). The magnetic field intensity profiles in fast and slow magnetic clouds, however, are very different, with strong evidence of compression in fast events and a more symmetric, force-free profile in slower events. This is likely to be the result of heliospheric dynamics rather than a signature of the formation process. Non-cloud ICMEs exhibit weaker magnetic field intensities than magnetic clouds, but there is little difference between fast and slow non-cloud ICMEs, except for some compression near the leading edge of fast non-clouds. The plasma properties of ICMEs – proton speed, density and temperature – are more strongly correlated with ICME speed than by ICME type (*i.e.* magnetic cloud or non-cloud classification). This is, again, largely due to similar levels of expansion during the ICME transit from the Sun to 1 AU.

In terms of heavy ion properties, fast magnetic clouds are clearly distinct from other ICME types. O and Fe charge states, as well as alpha-to-proton and Fe:O abundance ratios, are significantly enhanced above slow magnetic clouds and non-cloud ICMEs. This likely accounts for the observed correlation between geoeffectiveness and ICME ion charge states (Owens, Lockwood, and Barnard, 2018). The Fe charge state is better correlated with ICME speed than with ICME type (*i.e.* whether it is a magnetic cloud or not), while O charge states are better correlated with ICME type than speed. This is suggestive of extended heating through the corona being more important that impulsive heating in the low corona in producing fast ejecta. All ICMEs show an enhancement of C charge states near the ICME trailing edge, though this is most marked in magnetic clouds. It is unclear at present what causes this signature. It is unlikely to be associated with prominence material, which is expected to be anomalously cold (Burlaga *et al.*, 1998).

Fast ICMEs (both magnetic cloud and non-cloud) are embedded within faster, less dense ambient solar wind. This could be either cause or effect; slow ICMEs may be intrinsically linked to slow wind release mechanism and hence occur in close spatial proximity. Equally, ICMEs released into slower, denser ambient solar wind are expected to be slower and denser at 1 AU (regardless of initial conditions) due to increased drag (Cargill, 2004; Vrsnak and Gopalswamy, 2002). We note that the temperature and magnetic field intensity in the ambient solar wind ahead of fast ICMEs is not particularly suggestive of the fast, coronal-hole wind. Thus fast ICMEs may instead be more associated with multiple, compound events, which are able to further reduce the drag force on ejecta.

Disclosure of Potential Conflicts of Interest   The author declares to have no conflicts of interest.

References

Boe, B., *et al.*: 2018, *Astrophys. J.* **859**, 155. DOI.

Borrini, G., Gosling, J.T., Bame, S.J., Feldman, W.C.: 1983, *Solar Phys.* **83**, 367. DOI.

Burlaga, L.F.: 1988, *J. Geophys. Res.* **93**, 7217. DOI.

Burlaga, L.F., Sittler, E., Mariani, F., Schwenn, R.: 1981, *J. Geophys. Res.* **86**, 6673.

Burlaga, L., *et al.*: 1998, *J. Geophys. Res.* **10**, 277. DOI.

Cane, H.V., Richardson, I.G.: 2003, *J. Geophys. Res.* 108(A4). DOI.

Cargill, P.J.: 2004, *Solar Phys.* **221**, 135.

Chree, C., Stagg, J.M.: 1928, *Phil. Trans. Roy. Soc. London Ser. A* **227**, 647. DOI.

Crooker, N.U., Gosling, J.T., Smith, E.J., Russell, C.T.: 1990, *Physics of Magnetic Flux Ropes*, *Washington DC American Geophysical Union Geophysical Monograph Series* **58**.

Crooker, N.U., Burton, M.E., Siscoe, G.L., Kahler, S.W., Gosling, J.T., Smith, E.J.: 1996, *J. Geophys. Res.* **101**, 24331. DOI.

Ding, A., Habbal, S.R.: 2017, *Astrophys. J. Lett.* **842**, L7. DOI.

Eselevich, V.G., Fainshtein, V.G., Rudenko, G.V.: 1999, *Solar Phys.* **188**, 277. DOI.

Geiss, J., Gloeckler, G., von Steiger, R.: 1995, *Space Sci. Rev.* **72**, 49. DOI.

Gloeckler, G., *et al.*: 1998, *The Advanced Composition Explorer Mission*, Springer, Berlin 497.

Gloeckler, G., *et al.*: 1999, *Geophys. Res. Lett.* **26**, 157. DOI.

Gloeckler, G., Zurbuchen, T.H., Geiss, J.: 2003, *J. Geophys. Res.* 108(A4). DOI.

Gonzalez, W.D., *et al.*: 1998, *Geophys. Res. Lett.* **25**, 963. DOI.

Gosling, J.T.: 1993, *J. Geophys. Res.* **98**, 18937. DOI.

Gosling, J.T., Eriksson, S., McComas, D.J., Phan, T.D., Skoug, R.M.: 2007, *J. Geophys. Res.* 112(A8). DOI.

Gosling, J.T., Riley, P., McComas, D.J., Pizzo, V.J.: 1998, *J. Geophys. Res.* **103**, 1941. DOI.

Gruesbeck, J.R., Lepri, S.T., Zurbuchen, T.H., Antiochos, S.K.: 2011, *Astrophys. J.* 730. DOI.

Henke, T., *et al.*: 1998, *Geophys. Res. Lett.* **25**, 3465. DOI.

Kepko, L., Viall, N.M., Antiochos, S.K., Lepri, S.T., Kasper, J.C., Weberg, M.: 2016, *Geophys. Res. Lett.* **43**, 4089. DOI.

Landi, E., Gruesbeck, J., Lepri, S.T., Zurbuchen, T.H., Fisk, L.: 2012, *Astrophys. J.* 761. DOI.

Lepping, R.P., Jones, J.A., Burlaga, L.F.: 1990, *J. Geophys. Res.* **95**, 11957. DOI.

Lepri, S.T., Zurbuchen, T.H.: 2004, *J. Geophys. Res.* 109(A1). DOI.

Lepri, S.T., Zurbuchen, T.H., Fisk, L.A., Richardson, I.G., Cane, H.V., Gloeckler, G.: 2001, *J. Geophys. Res.* **106**, 29231. DOI.

Lepri, S.T., Laming, J.M., Rakowski, C.E., Von Steiger, R.: 2012, *Astrophys. J.* **760**, 2. DOI.

Low, B.C.: 2001, *J. Geophys. Res.* **106**, 25141. DOI.

Luhmann, J.G., Larson, D., Hoeksama, J.T., Zhao, X.-P., Arge, C.N., Cyr, O.C.St.: 1999 In: *Solar Wind Nine* **725**.

McComas, D.J., *et al.*: 1998, *Space Sci. Rev.* **86**, 563. DOI.

McComas, D.J., Elliott, H.A., Schwadron, N.A., Gosling, J.T., Skoug, R.M., Goldstein, B.E.: 2003, *Geophys. Res. Lett.* 30(10). DOI.

Owens, M.J., Cargill, P.J.: 2002, *J. Geophys. Res.* **107**, SSH 1-1. DOI.

Owens, M.J., Cargill, P.J.: 2004, *Ann. Geophys.* **22**, 661. DOI.

Owens, M.J., Cargill, P.J., Pagel, C., Siscoe, G.L., Crooker, N.U.: 2005, *J. Geophys. Res.* 110(A1). DOI.

Owens, M.J., Crooker, N.U.: 2006, *J. Geophys. Res.* 111(A10). DOI.

Owens, M.J., Forsyth, R.J.: 2013, *Living Rev. Solar Phys.* **10**, 5. DOI.

Owens, M.J., Lockwood, M., Davis, C.J., Barnard, L.: 2011, *Geophys. Res. Lett.* 38(19). DOI.

Owens, M.J., Merkin, V.G., Riley, P.: 2006, *J. Geophys. Res.* 111(A3). DOI.

Owens, M.J., Lockwood, M., Barnard, L.A.: 2018, *Space Weather* **16**, 694. DOI.

Owocki, S.P., Holzer, T.E., Hundhausen, A.J.: 1983, *Astrophys. J.* **275**, 354. DOI.

Pizzo, V.J.: 1991, *J. Geophys. Res.* **96**, 5405. DOI.

Priest, E.R.: 1982, *Solar Magnetohydrodynamics*, Reidel, Dordrecht.

Riley, P., *et al.*: 2004, *J. Atmos. Solar-Terr. Phys.* **66**, 1321.

Riley, P., Schatzman, C., Cane, H.V., Richardson, I.G., Gopalswamy, N.: 2006, *Astrophys. J.* **647**, 1. DOI.

Russell, C.T., Mulligan, T.: 2002, *Planet. Space Sci.* **50**, 527.

Shen, C., Raymond, J.C., Mikić, Z., Linker, J.A., Reeves, K.K., Murphy, N.A.: 2017, *Astrophys. J.* 850. DOI.

Smith, C.W., L'Heureux, J., Ness, N.F., Acuna, M.H., Burlaga, L.F., Scheifele, J.: 1998, *Space Sci. Rev.* **86**, 613. DOI.

Song, H., *et al.*: 2016, *Astrophys. J. Suppl.* **224**, 2. DOI.

Song, H., *et al.*: 2017, *Astrophys. J. Lett.* **836**, 1. DOI.

von Steiger, R., *et al.*: 2000, *J. Geophys. Res.* **105**, 27217. DOI.

Vrsnak, B., Gopalswamy, N.: 2002, *J. Geophys. Res.* **107**, SSH 2-1. DOI.

Yohei, Y., Suess, S.T., Steinberg, J.T., Takashi, S.: 2004, *J. Geophys. Res.* 109(A3). DOI.

Zhao, L., Landi, E., Zurbuchen, T., Fisk, L., Lepri, S.: 2014, *Astrophys. J.* 793(1). DOI.

Zirker, J.B.: 1977, *Rev. Geophys.* **15**, 257.

Zurbuchen, T.H., Fisk, L., Lepri, S., von Steiger, R.: 2003, The composition of interplanetary coronal mass ejections. In: *AIP* **604**.